# Single-site cobalt catalyst embedded in a covalent triazine-based framework (CTF) for photocatalytic $CO_2$ reduction

Anupam Jana,[a] Arijit Maity,[a] Abhimanyu Sarkar,[a] Bibhutibhushan Show,[a] Preeti A. Bhobe[b] and Asamanjoy Bhunia*[a]

[a.]Department of Chemistry, Inorganic Chemistry Section, Jadavpur University, Kolkata 700032, India.
[b.]Department of Physics, Indian Institute of Technology Indore, Indore 453552 Madhya Pradesh, India
* Corresponding author: E-mail: ahunia.chemistry@jadavpuruniversity.in

## Electronic Supplementary Information (ESI)

### Experimental Section

### Materials: Chemicals

$CF_3SO_3H$, and TEOA were purchased from Sigma-Aldrich. DCM, Acetone, Acetonitrile, THF, and Chloroform were purchased from Spectrochem. All solvents and chemicals were used without any further purification.

### Characterization methods

Fourier transform–infrared (FT–IR) spectra of CTF-TPE and CTF-TPE@Co-n were collected on a Nicolet Magna IR 750 series-II FTIR spectrophotometer within the range of 400 $cm^{-1}$ to 4000 $cm^{-1}$ using KBr plates. The powder X-ray diffraction (PXRD) data of CTF-TPE and CTF-TPE@Co-n were collected with Bruker D8 Advance X-ray diffractometer (XRD) at room temperature using Cu Kα radiation (λ = 1.548 Å) in a 2θ range of 3–55°. Thermogravimetric analyses (TGA) were done at a ramp rate of 20 °C $min^{-1}$ under air with Perkin Elmer Pyris Diamond TG–DTA instruments. UV absorption spectra were recorded using a Cary 60 UV–vis (Agilent Technologies) with a 1 cm path-length quartz cell. Fluorescence emission spectra were collected on a HORIBA Fluoromax-4 fluorometer. Nitrogen gas adsorption–desorption of the samples was performed to obtain BET-specific surface area (SBET) using Quanta chrome Autosorb iQ2 Instruments at liquid $N_2$ temperature (77 K). The samples were degassed under a high vacuum ($10^{-6}$ torr) at 105 °C for 10 h. After degassing, the sample tube was then transferred

to the analysis port of the sorption analyzer. Pore size distribution was calculated by quenched solid density functional theory (QSDFT) slit/cylindrical pore model. $^{1}H$ and $^{13}C$ NMR spectra were measured on Bruker-DRX 400 MHz instruments at room temperature in $CDCl_3$. Field emission scanning electron microscope (FE-SEM) images with elemental mapping were obtained using a Carl Zeiss SUPRA 55VP FESEM instrument. Energy dispersive X-ray spectroscopy (EDS) was performed by Oxford Instruments X-Max with INCA software coupled to the FE-SEM. The Hitachi, S-4800, EDS detector was introduced to analyze the morphology and EDS of the samples. The Electron Paramagnetic Resonance (EPR) experiments were conducted with a JEOL JESFA200 ESR Spectrometer instrument having an X-band Microwave unit. The High-resolution transmission electron microscopy (HR-TEM) images were collected from the JEM, JEM-2100F instrument, operating at an accelerating voltage of 200 kV. Before the analysis, the 2-propanol solution of a small amount of sample was dispersed homogeneously in an ultrasonic cleaner for 2 h to ensure maximum dispersion of the sample, and then 2 µL of the solution was cast on a carbon-coated Cu-grid (300 mesh size), put in an airtight desiccator, and dried at ambient temperature for two days. HAADF-STEM and the corresponding EDS mapping were recorded using the same instrument. X-ray photoelectron spectroscopy (XPS) measurement was conducted by the Thermo Fisher ESCALAB Xi+ microProbe instrument with a monochromatic Al-Kα target, 1486.6 eV energy, and a maximum power of 15.0 KW. CoK-edge EXAFS measurement was carried out using the RIGAKU R-XAS laboratory spectrometer equipped with a 3 kW X-ray source and Ge (220) monochromator. Data was recorded in the transmission mode using a gas-filled ionization chamber before the sample and a scintillation detector after the sample. Inductively coupled plasma optical emission spectrometry (ICP-OES) results were obtained from an Icap 7000 ICP-OES (Thermo Scientific). After the photocatalysis, gaseous and liquid products were analyzed. The gaseous product was analyzed and quantified using TCD and FID detector in High-performance gas chromatography (Agilent 8860). GC was calibrated with known standard for $H_2$, CO and $CH_4$. Liquid products were analysed on a Metrohm Eco IC and $^{1}H$ NMR. For the isotope labeling experiment, we purged the reaction mixture with $^{13}CO_2$. This product was detected using gas chromatography by MS detector (Perkin Elmer clarus 690).

**Synthesis of tetra(4-bromophenyl)ethylene:**

Bromine (8.8 mL, 170 mmol) was added over a 10 min period to a solution of tetraphenyl ethylene (7.2 g, 21.7 mmol) in 40 mL of glacial acetic acid bathed in the ice water. After further adding dichloromethane (30 mL), the resulting mixture was heated at 50 ℃ for about 30 min [based on thin layer chromatography (TLC) detection]. The reaction mixture was added to 200 mL of ice water, and the precipitated solid was filtered and washed repeatedly with water and ethanol. The yield of crude product was 12.2 g (87%). The product was used directly without further purification. $^1$H NMR ($CDCl_3$, 500 MHz) δ (ppm): 7.27 (d, J = 8.5 Hz, 8H) and 6.85 (d, J = 8.5 Hz, 8H).

**Synthesis of tetra(4-cyanophenyl) ethylene (2).**

Tetra(4-bromophenyl) ethylene (6.5 g, 10.0 mmol), CuCN (5.0 g, 55.9 mmol), and DMF (50 mL) were placed in a 150 mL Schlenk flask. The mixture was heated at reflux for 60 h under a nitrogen atmosphere and then suspended in 300 mL water. Ethylenediamine (10 mL) was added, and the resulting mixture was stirred at 100 °C for 1 h and filtered. The precipitated solid was extracted with dichloromethane (3 × 150 mL each). The combined organic phase was dried with $MgSO_4$, filtered, and evaporated in a vacuum. The residue was repeatedly purified by chromatography on silica using a hexane/$CH_2Cl_2$ (1:1) as eluent, giving tetra(4-cyanophenyl) ethylene 3.2 g with a yield of 74%. $^1$H NMR ($CDCl_3$, 500 MHz) δ (ppm): 7.48 (t, J = 5.0 Hz, 8H) and 7.08 (t, J = 5.0 Hz, 8H).

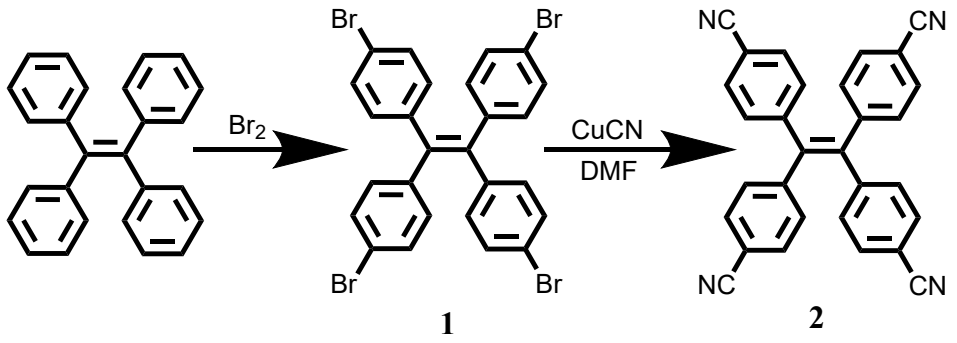


**Scheme S1:** Synthesis of the nitrile linker.

**Electrochemical characterization:**

The Mott-Schottky analysis and impedance measurement were conducted using CHI760E workstation (CHI Instruments, USA) through a conventional three-electrode system immersed in a 0.2 M $Na_2SO_4$ aqueous solution.

**Preparation of working electrode for Mott-Schottky measurement:**

2.5 mg of respective CTF materials were dispersed in a solution of 250 µL water, 250 µL isopropyl alcohol (IPA), and 10 µL of Nafion to prepare a homogenous slurry. Subsequently, 12 µL of slurry was coated on a glassy carbon electrode and then dried at room temperature. The Ag/AgCl electrode was employed as the reference electrode, and the platinum plate was used as the counter electrode, respectively. The measurements were carried out under frequencies of 0.5, 1, and 1.5 kHz.

**Preparation of working electrode for impedance measurement:**

2.5 mg of respective CTF materials were dispersed in a solution of 250 µL water, 250 µL isopropyl alcohol (IPA), and 10 µL of Nafion to prepare a homogenous slurry. Subsequently, 12 µL of slurry was coated on a glassy carbon electrode and then dried at room temperature. The Ag/AgCl electrode was employed as the reference electrode, and the platinum plate was used as the counter electrode, respectively. A 0.2 M $Na_2SO_4$ solution was used as an electrolyte. The measurements were carried out with a bias potential of -0.4 V with a frequency range from $10^{-2}$ to $10^5$ Hz under a nitrogen atmosphere.

**Preparation of working electrode for transient photocurrent:**

2.5 mg of respective CTF materials was dispersed in a solution of 250 µL water, 250 µL isopropyl alcohol (IPA), and 10 µL of Nafion to prepare a homogenous slurry. Subsequently, 300 µL of slurry was coated on an FTO glass plate (1 cm × 1 cm) and then dried at room temperature. The Ag/AgCl electrode was employed as the reference electrode, and the platinum plate was used as the counter electrode, respectively. The transient photocurrent responses were carried out under visible-light irradiation conditions (300 W Xenon arc lamp).

**Photocatalytic testing:**

The photocatalytic reactions were conducted with a 275 W Xe lamp with a 420 nm cut-off filter was used as the light source. In a typical process, a specific amount (~2 mg) of catalyst, 2,2'-bipyridine (9.3 mg) as a cocatalyst, and $[Ru(bpy)_3]Cl_2 \cdot 6H_2O$ (10.4 mg) was dispersed into the solution of 3.0 mL acetonitrile solution containing TEOA and $H_2O$ (acetonitrile: TEOA: $H_2O$= 3:1:1 v/v) in a quartz test tube. Before photocatalytic testing, the reaction solution was degassed with $N_2$ gas for 20 minutes followed by bubbling with $CO_2$ (99.999%, Airgas) in the dark for 30 min. The reaction solution was then irradiated at room temperature with stirring for photocatalytic $CO_2$ reduction (see Figure S20). The headspace above the reaction solution was taken using a gas-tight syringe at different time intervals for product analysis using an Agilent 8860 equipped with a TCD and FID detector and a 60/80 Carboxen-1000 packed column (Supelco). The experimental component and amount of gas product were identified using the standard gas. Control experiments were conducted in the absence of light irradiation, photosensitizer, catalyst, sacrificial reagent, and $CO_2$. Isotope-labeled experiments were conducted with $^{13}CO_2$ instead of $^{12}CO_2$ under the same condition, and the obtained gaseous products were analyzed by gas chromatography−mass spectrometry (GC-MS). Liquid products were analysed using ion chromatography and $^1H$ NMR.

**Table S1**: Comparison of CO evolution by different Co-loaded photocatalysts

| Photocatalyst | Co loading (wt%) | CO product (μmol/gm) | $H_2$ product (μmol/gm) |
|---|---|---|---|
| CTF-TPE@Co-1 | 0.8 | 565 | 245 |
| CTF-TPE@Co-2 | 1.5 | 1113 | 877 |
| **CTF-TPE@Co-3** | **3.1** | **1515** | **938** |
| ***CTF-TPE@Co-3** | **3.1** | **6616** | **5978** |
| CTF-TPE@Co-4 | 5.9 | 1172 | 1178 |

*Long photocatalytic run for 7 hours

**FT-IR:**

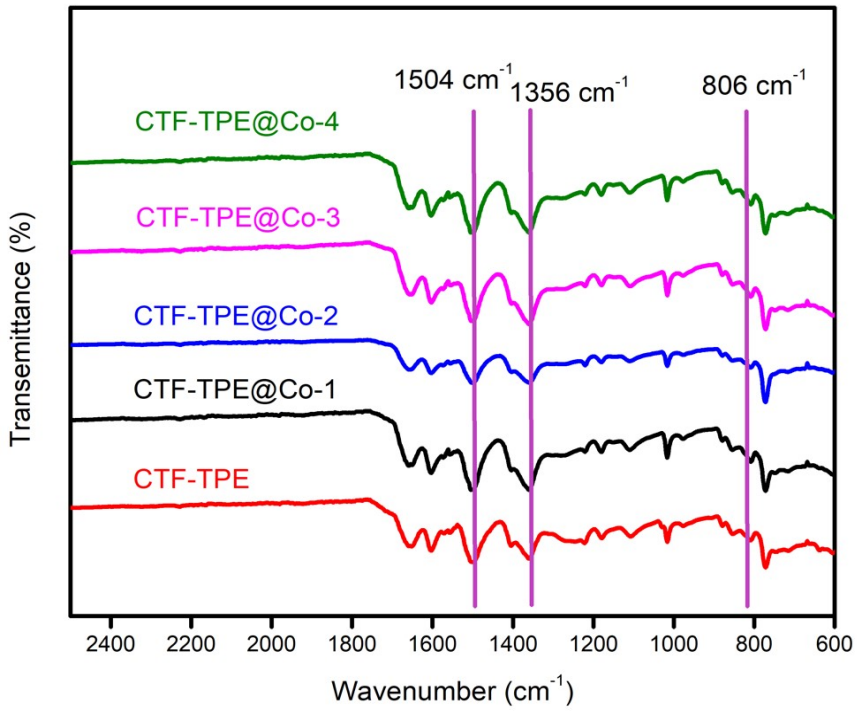


Fig. S1: Comparison of IR-spectra of different CTF-TPE@Co.

**Thermogravimetric Analysis (TGA):**

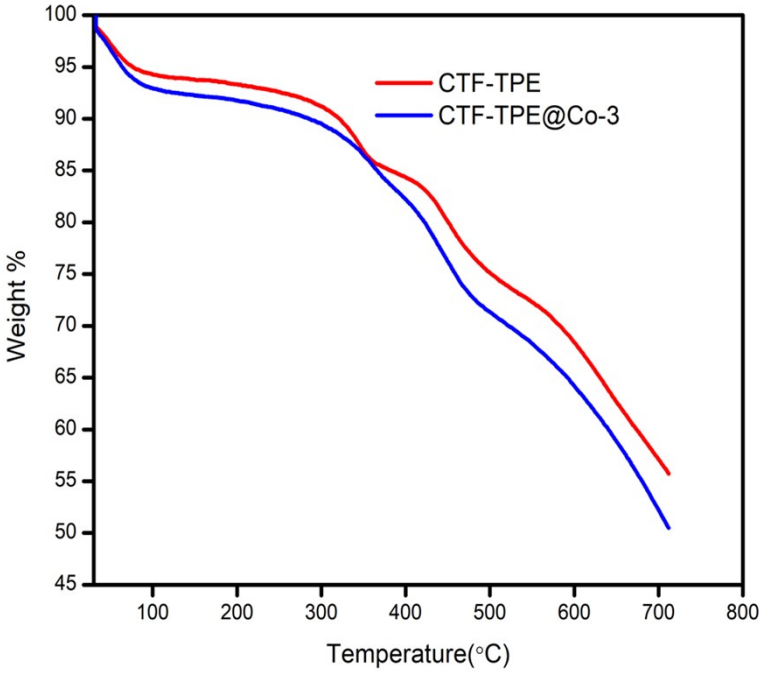


Fig. S2: TGA for CTF-TPE and CTF-TPE@Co-3 in temperature range of 30 to 800 °C at the heating rate of 5 °C/min under $N_2$ atmosphere.

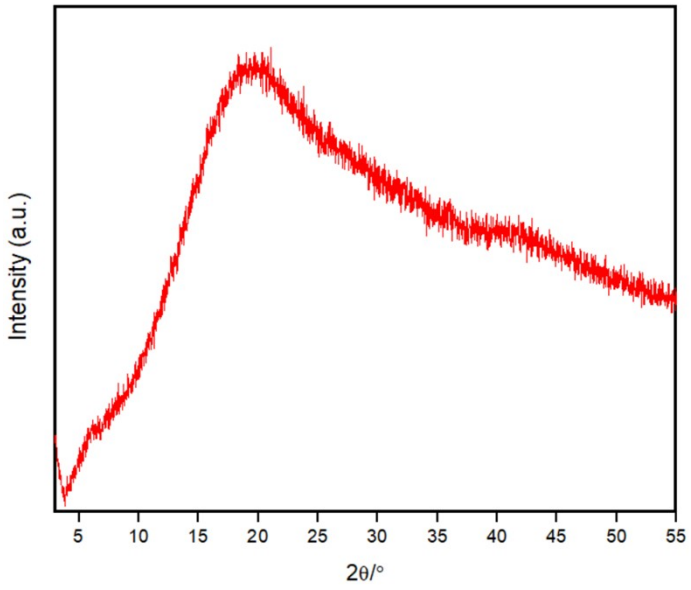


Fig. S3: PXRD pattern of CTF-TPE@Co-4 (high loading of Co metal).

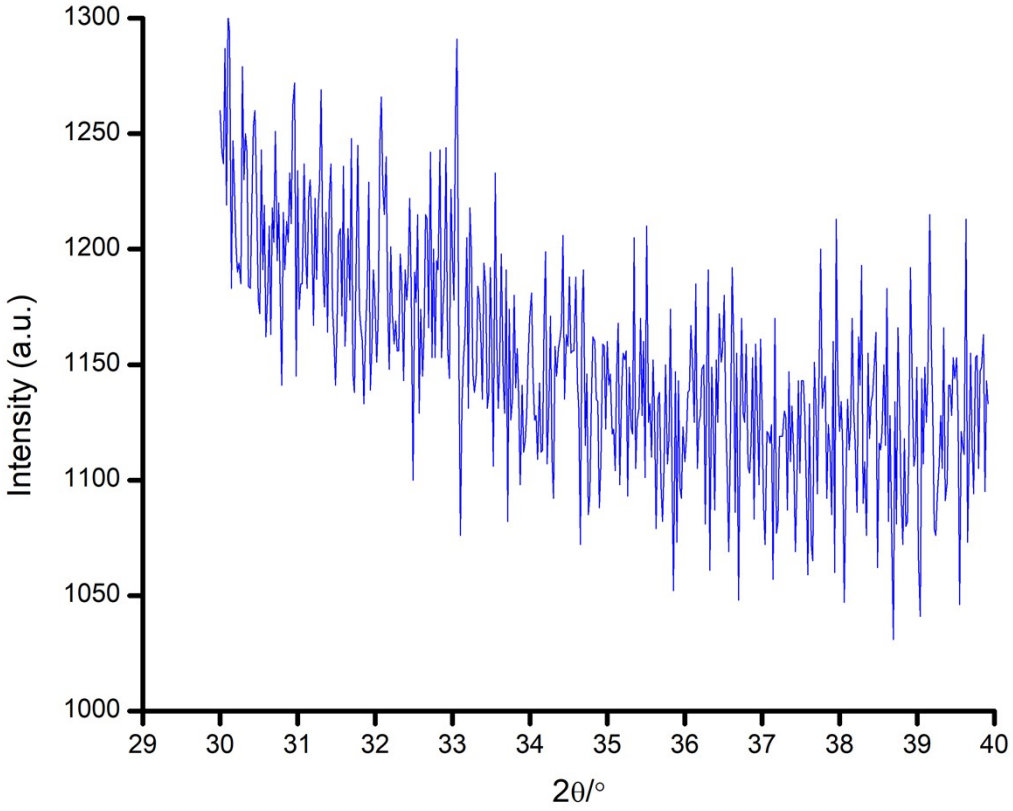


Fig. S4: PXRD profile at a very high scan rate.

Table S2: BET, Langmuir surface area, pore size and pore volume measurements:

| SL No | Sample Name | BET surface area ($m^2g^{-1}$)[a] | Langmuir surface area ($m^2g^{-1}$)[b] | Pore size (nm)[c] | Pore volume ($cm^3g^{-1}$) |
|---|---|---|---|---|---|
| 1. | CTF-TPE | 434 | 597 | 0.43 | 0.27 |
| 2. | CTF-TPE@Co-3 | 243 | 273 | 0.39 | 0.17 |

[a]BET surface area derived from the $N_2$ adsorption isotherm at 77 K over the relative pressure range $p/p_0$ = 0.01–0.05. [b]Langmuir surface area over the pressure range of 0–110 torr. [c]Pore size distribution measured by QSDFT.

**Pore size distribution:**

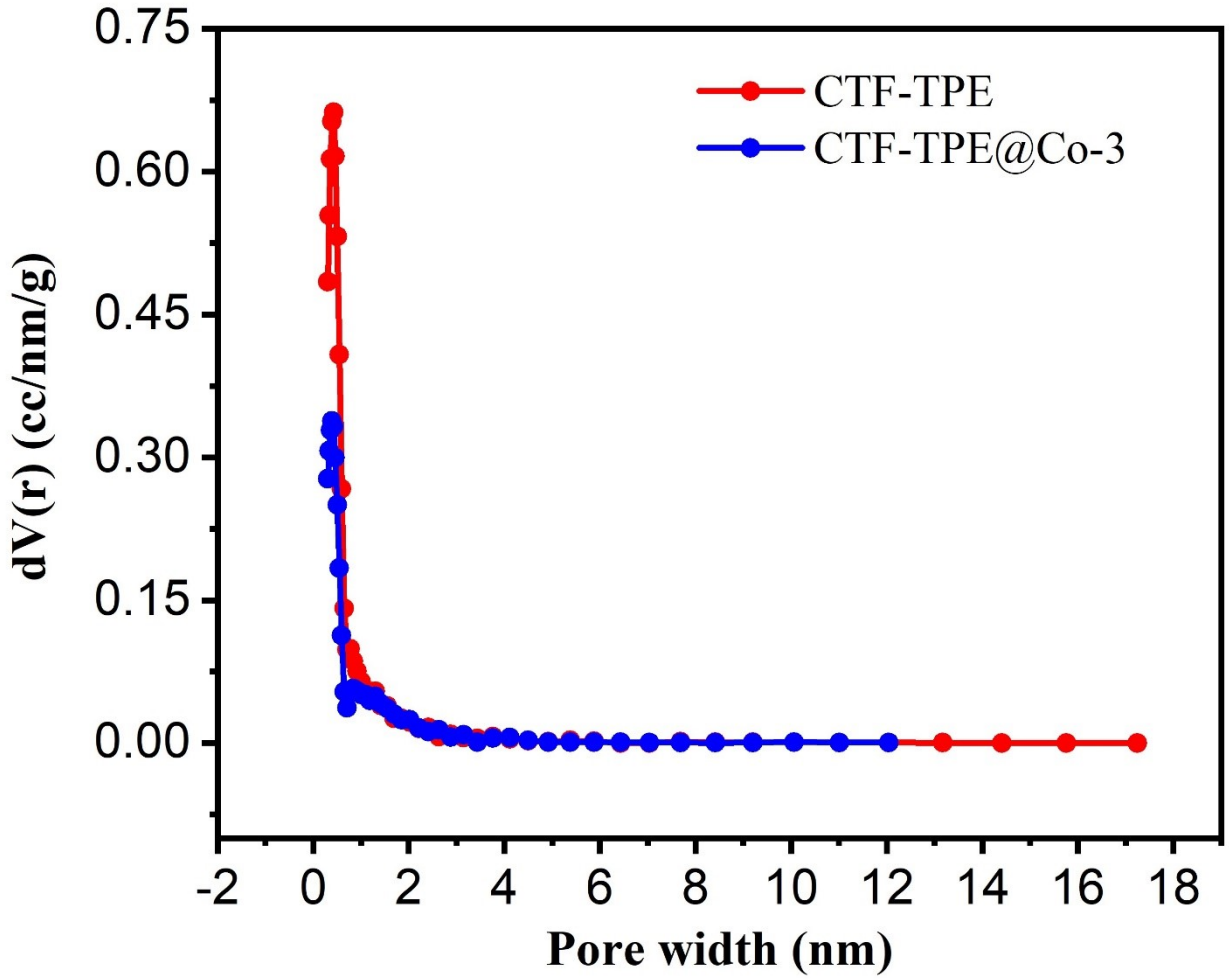


Fig. S5: Pore size distribution of CTF-TPE and CTF-TPE@Co-3 were evaluated using QSDFT method.

**XPS Spectra of CTF:**

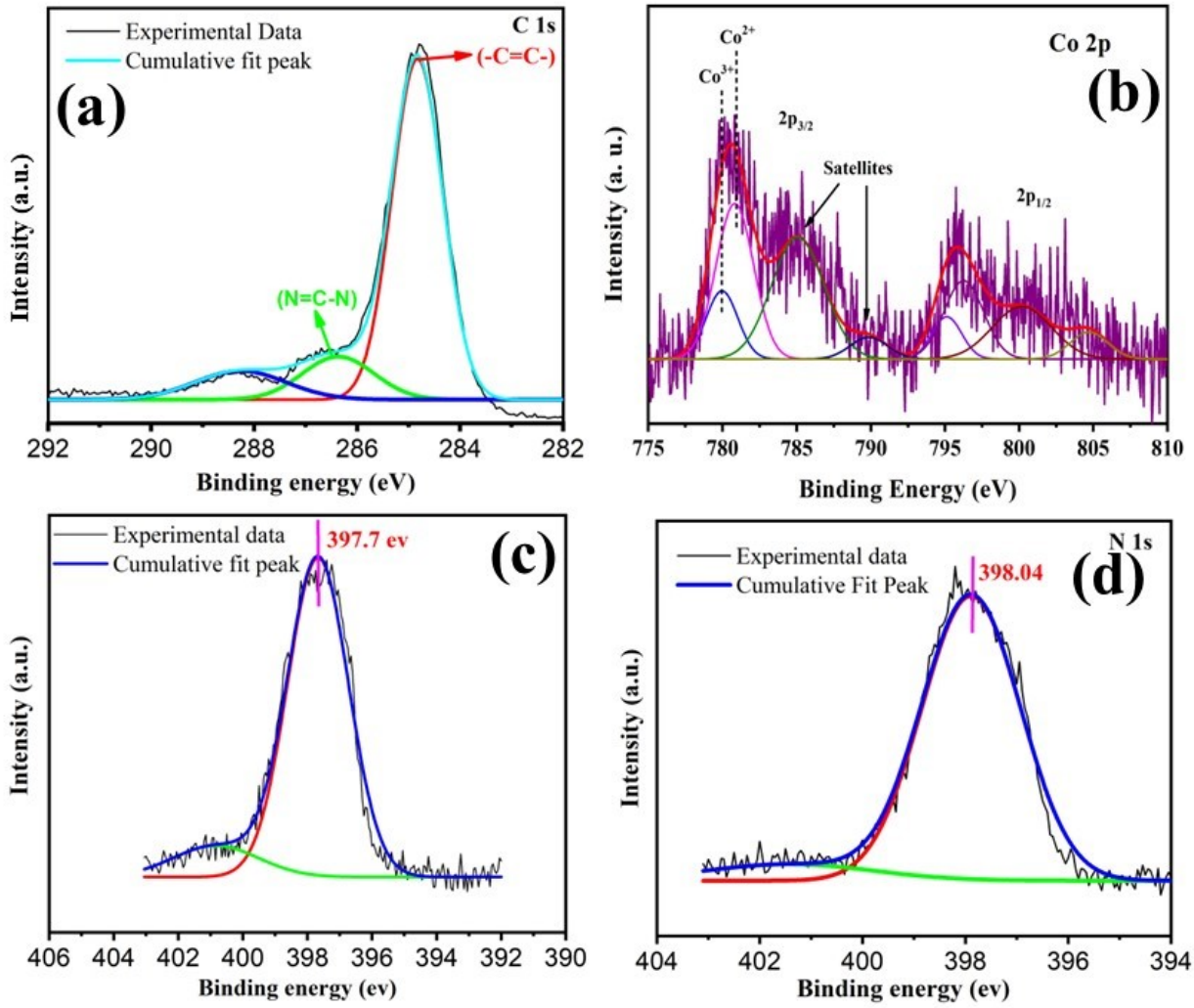


Fig. S6: XPS spectra (C 1s) of CTF-TPE (a); Co 2p of CTF-TPE@Co-3 (b); N 1s of CTF-TPE (c) and N 1s of CTF-TPE@Co-3 (d).

**ICP-OES Measurements:**

The cobalt content in the CTF-TPE@Co-n (n=1 to 4) materials were determined by inductively coupled plasma atomic emission spectrometer (ICP-AES). 2-3 mg of CTF-TPE@Co-n were digested in a 3% $HNO_3$ solution (0.5 ml) and heated in a Biotage SPX microwave reactor at 120 °C for 15 min. Afterwards, the solution became clear. The resulting acidic solution was diluted to 10 mL with deionized $H_2O$ and analyzed for Co.

Table S3: Amount (Wt%) of cobalt present in CTF-TPE@Co-n (n=1 to 4).

| **Catalyst** | **Wt% of Co** |
|---|---|
| CTF-TPE@Co-1 | 0.80 % |
| CTF-TPE@Co-2 | 1.50 % |
| CTF-TPE@Co-3 | 3.10 % |
| CTF-TPE@Co-4 | 5.90 % |

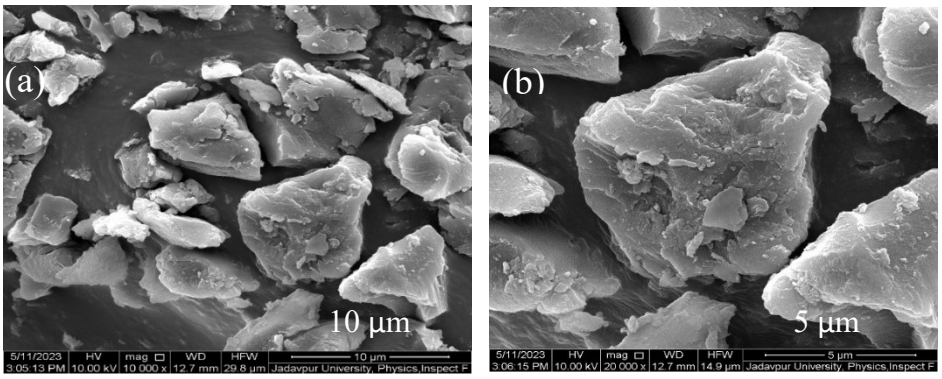


**Fig. S7**: SEM image of CTF-TPE@Co-3.

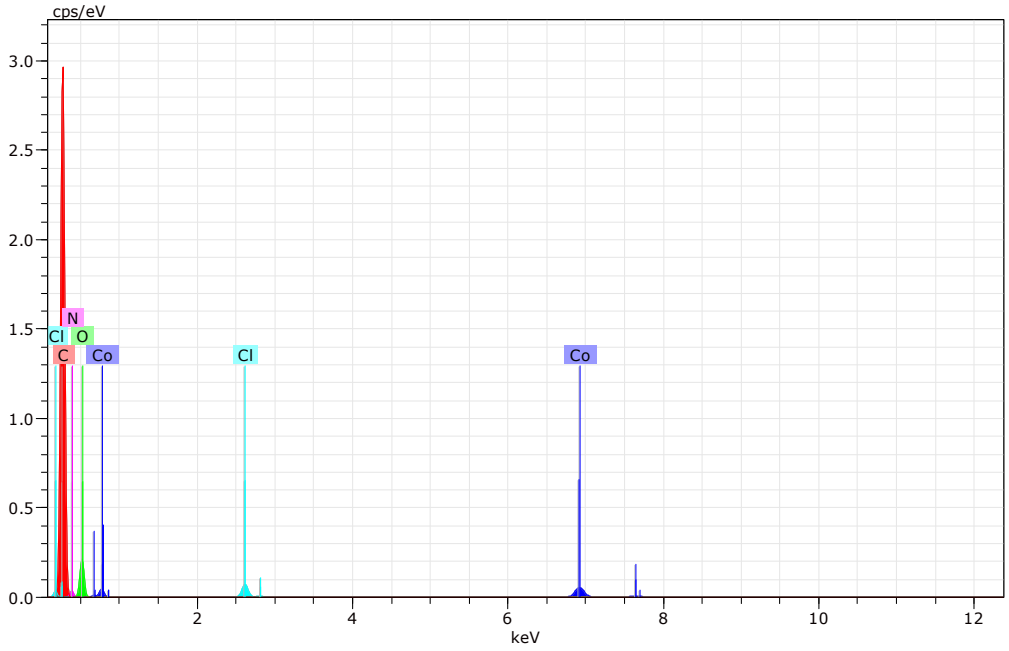


Spectrum: Acquisition 4750

| Element | unn. C [wt.%] | norm. C [wt.%] | Atom. C [at.%] | Compound norm. Comp. C [wt.%] | Error (3 Sigma) [wt.%] |
|---|---|---|---|---|---|
| Carbon | 0.00 | 0.00 | 0.00 | 0.00 | 0.00 |
| Oxygen | 9.25 | 71.74 | 77.38 | 71.74 | 7.26 |
| Cobalt | 1.29 | 10.04 | 2.94 | 10.04 | 0.30 |
| Chlorine | 0.48 | 3.73 | 1.82 | 3.73 | 0.18 |
| Nitrogen | 1.87 | 14.50 | 17.86 | 14.50 | 2.88 |
| Total: | 12.89 | 100.00 | 100.00 | | |

unn. C [wt.%] = the un-normalized concentration in weight percent of the element,
norm. C [wt.%] = the normalized concentration in weight percent of the element,
C Atom. [at.%] the atomic weight percent,
C Error (3 Sigma) [wt. %)] = the error in the weight percent concentration at the 3 sigma level.

Fig. S8: EDX of CTF-TPE@Co-3.

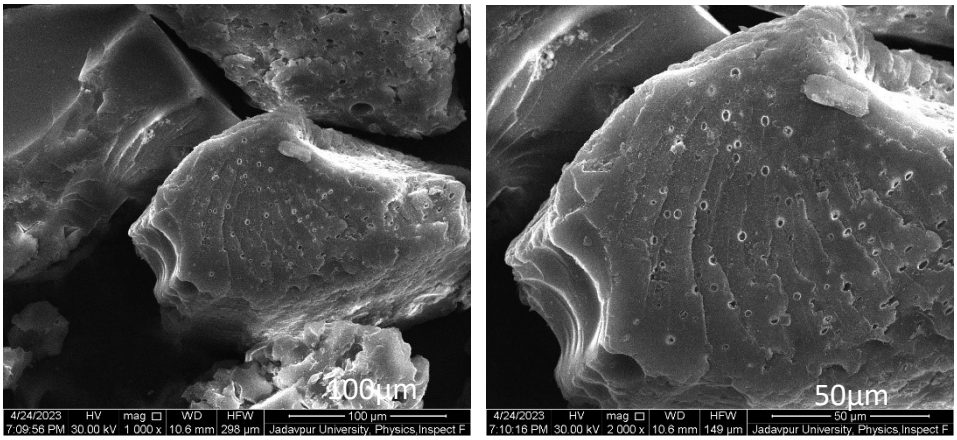


Fig. S9: SEM image of CTF-TPE@Co-4

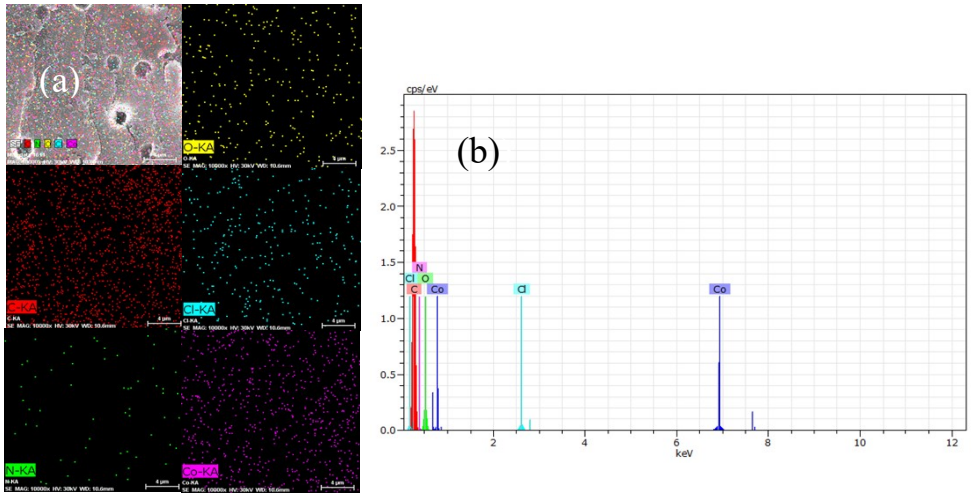


| Element | unn. C [wt.%] | norm. C [wt.%] | Atom. C [at.%] | Compound [wt.%] | norm. Comp. C [wt.%] | Error (3 Sigma) [wt.%] |
|---|---|---|---|---|---|---|
| Carbon | 0.00 | 0.00 | 0.00 | 0.00 | 0.00 | |
| Oxygen | 8.07 | 53.09 | 71.61 | 53.09 | 6.65 | |
| Cobalt | 5.34 | 35.12 | 12.86 | 35.12 | 0.68 | |
| Nitrogen | 1.36 | 8.95 | 13.80 | 8.95 | 2.74 | |
| Chlorine | 0.43 | 2.84 | 1.73 | 2.84 | 0.18 | |

Fig S10: Elemental mapping (a) and EDX of CTF-TPE@Co-4 (b).

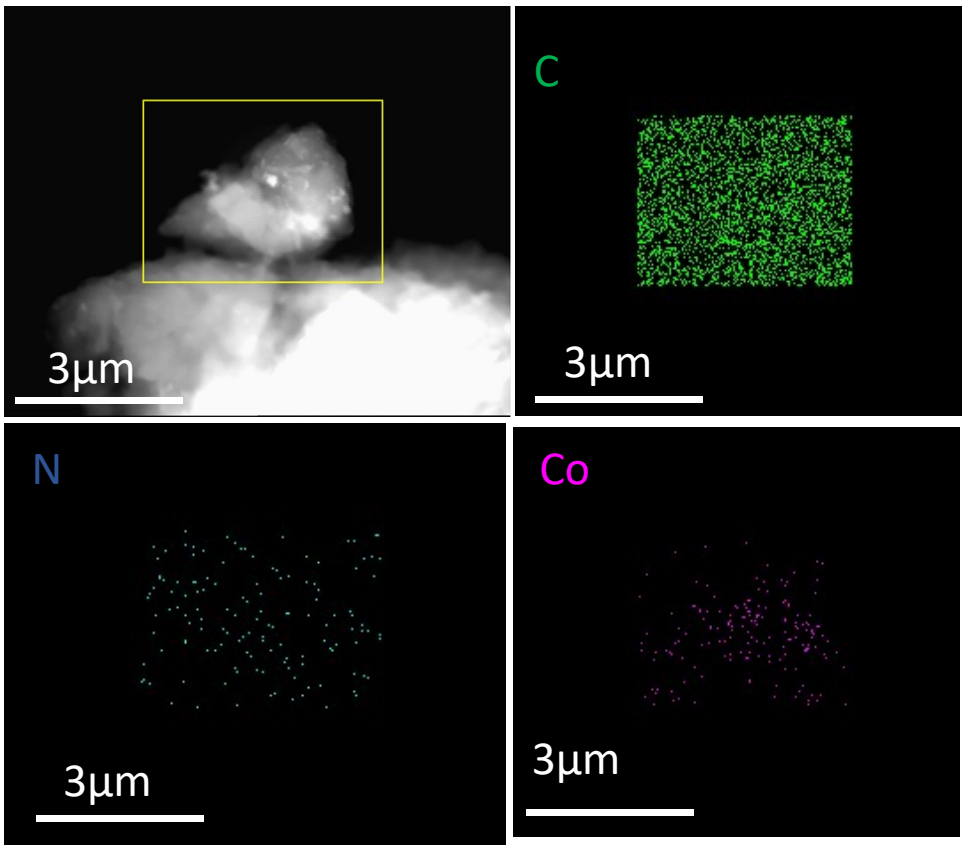


Fig. S11: EDX mapping images of C, N, Co elements in the CTF-TPE@Co-3.

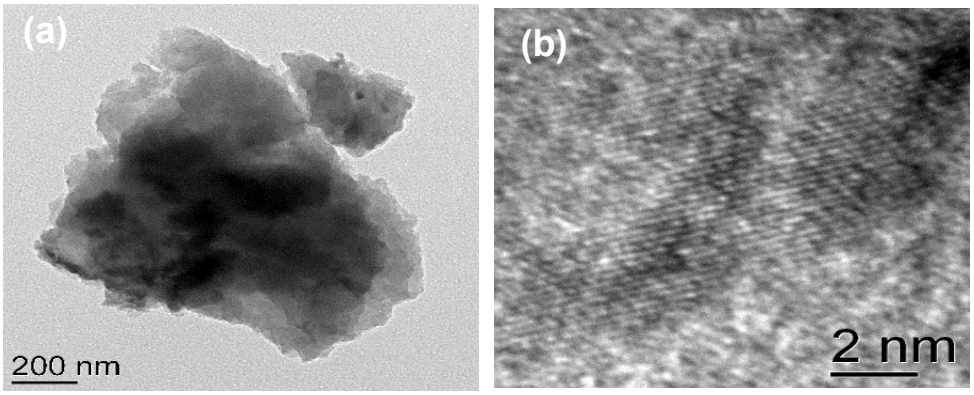


Fig. S12: HR-TEM image of CTF-TPE@Co-3.

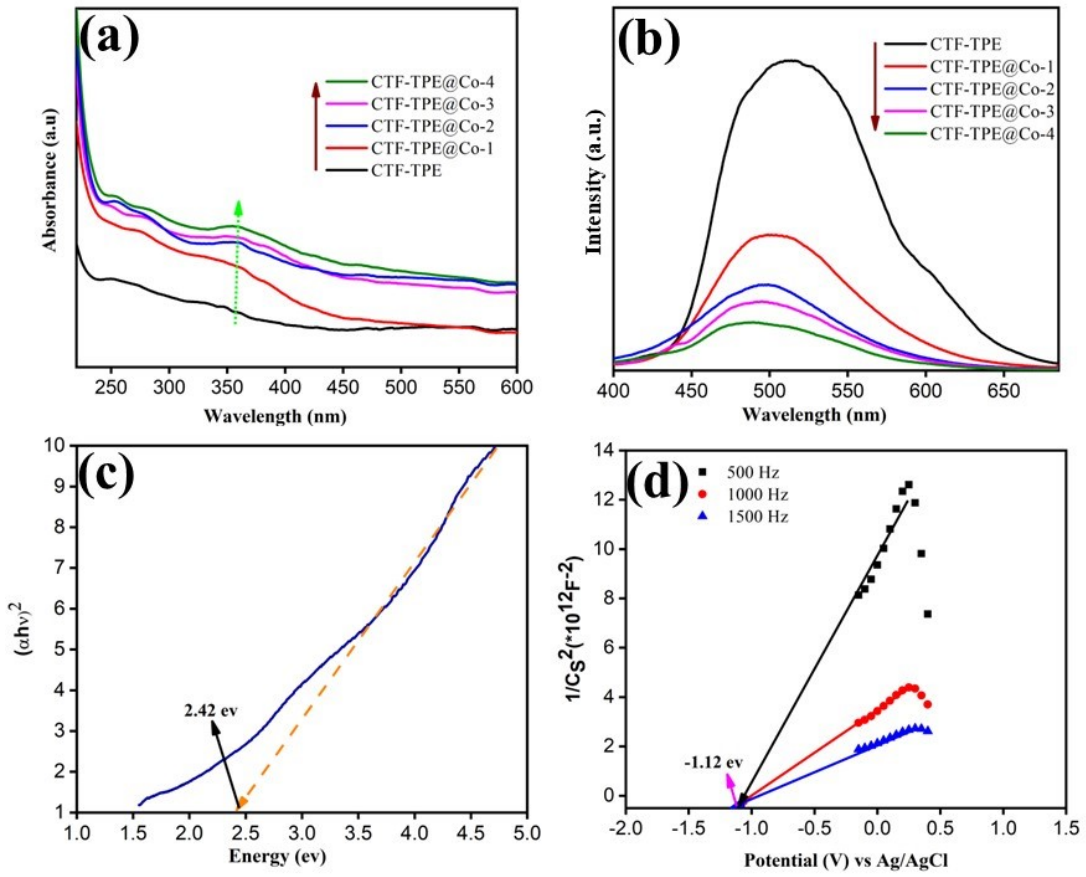


Fig. S13: (a) UV-VIS absorption spectra of CTF and CTF-TPE@Co-n (n= 1 to 4); (b)Fluorescence spectra of CTF-TPE and CTF-TPE@Co-n (n= 1 to 4); (c)Tauc plot for CTF-TPE@Co-3; (d) Mott-Schottky plots of CTF-TPE@Co-3 at different frequencies.

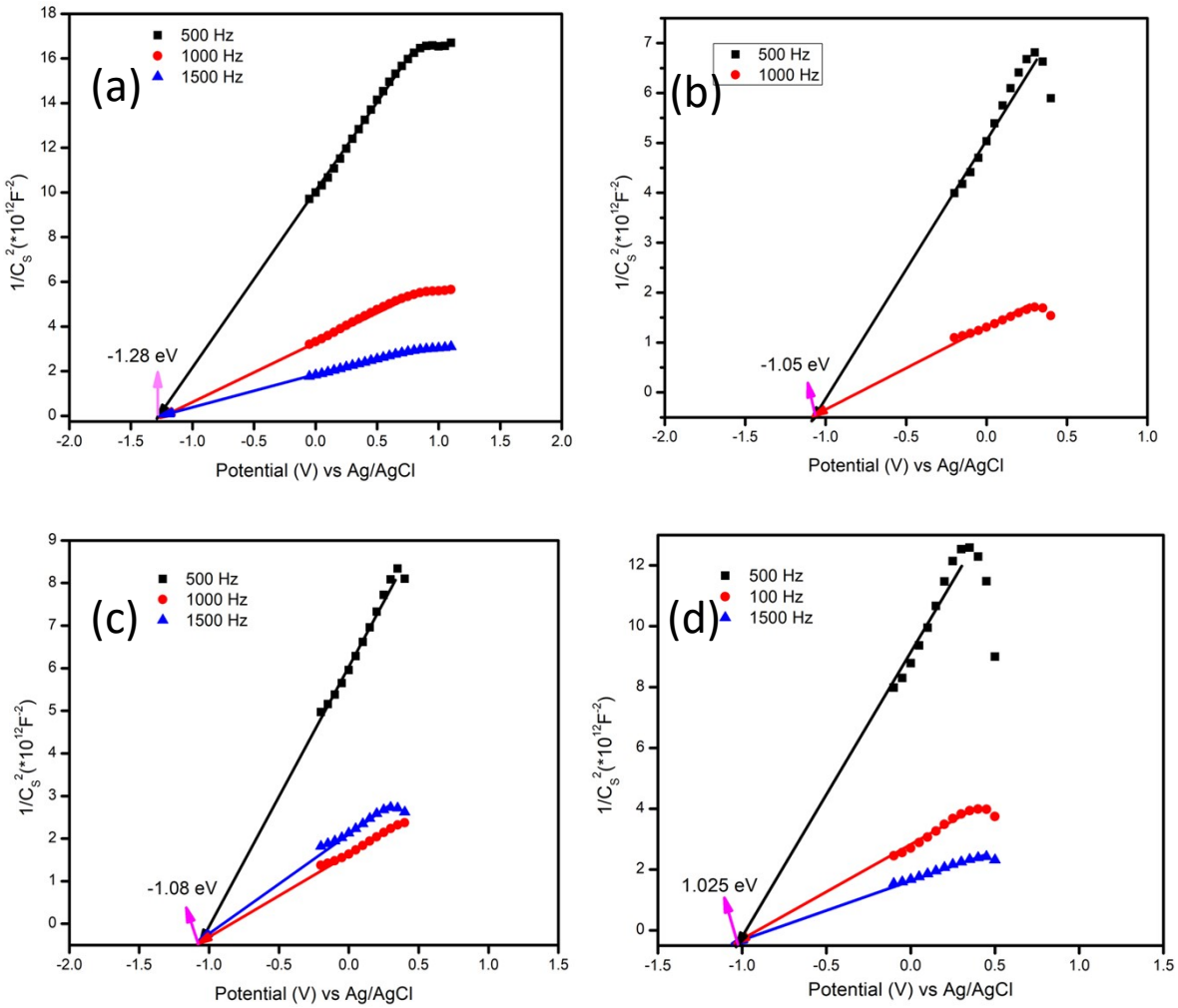


Fig. S14: Mott-Schottky plots of CTF-TPE, CTF-TPE@Co-1, CTF-TPE@Co-2, CTF-TPE@Co-4 at different frequency.

**Isotope labelling experiment:**

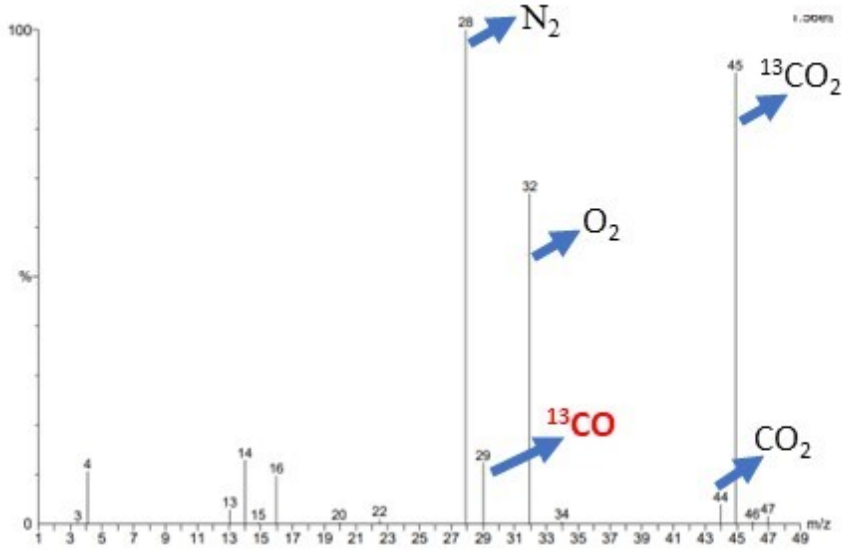


Fig. S15: Isotope labeling experiment in presence of $^{13}CO_2$.

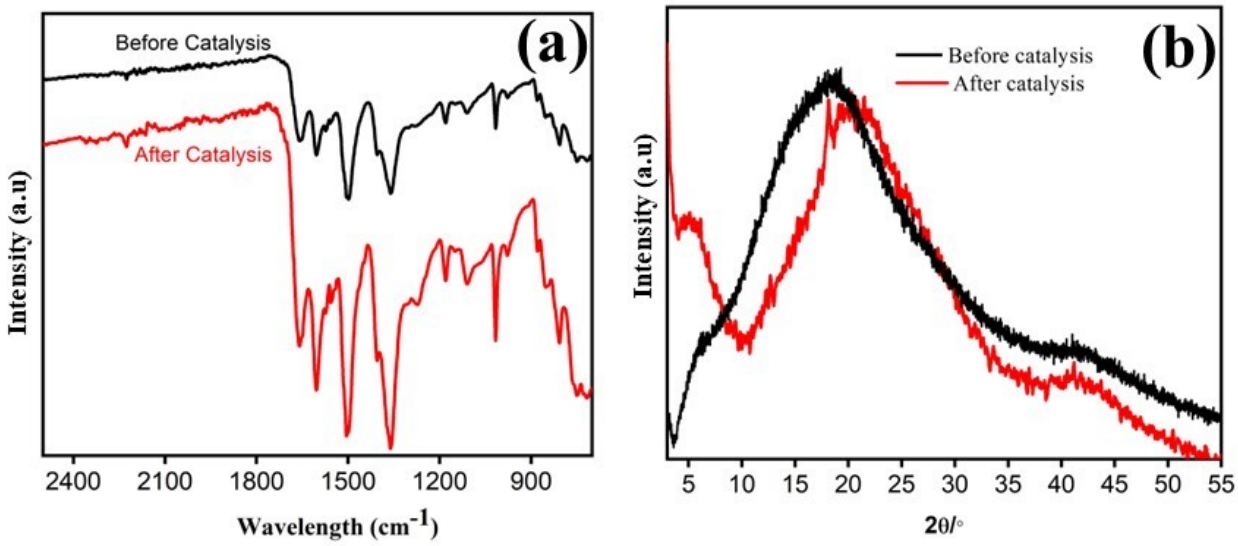


Fig. S16: (a) FT-IR spectra and; (b) PXRD profile of CTF-TPE@Co-3 before and after photocatalysis.

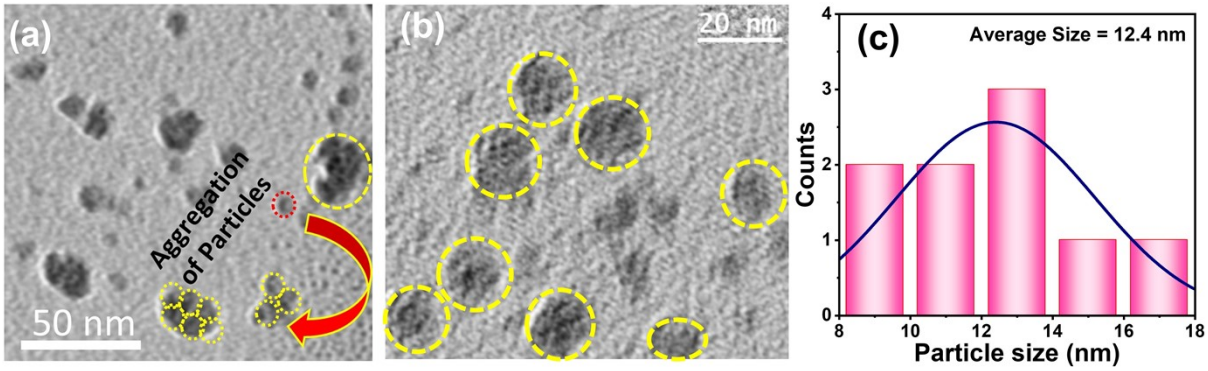


Fig. S17: HR-TEM image of CTF-TPE@Co-4. Highlighted parts are showing the formation of cobalt clusters through agglomeration. The average size of the particle is found to be 12.4 nm.

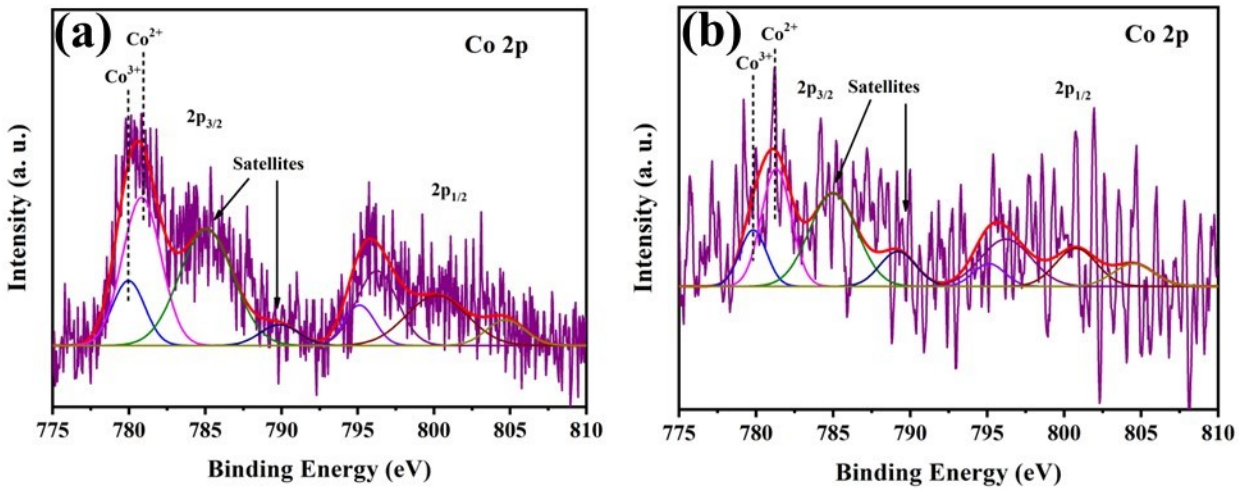


Fig. S18: (a) XPS spectra of Co 2p before catalysis. (b) XPS spectra of Co 2p after catalysis.

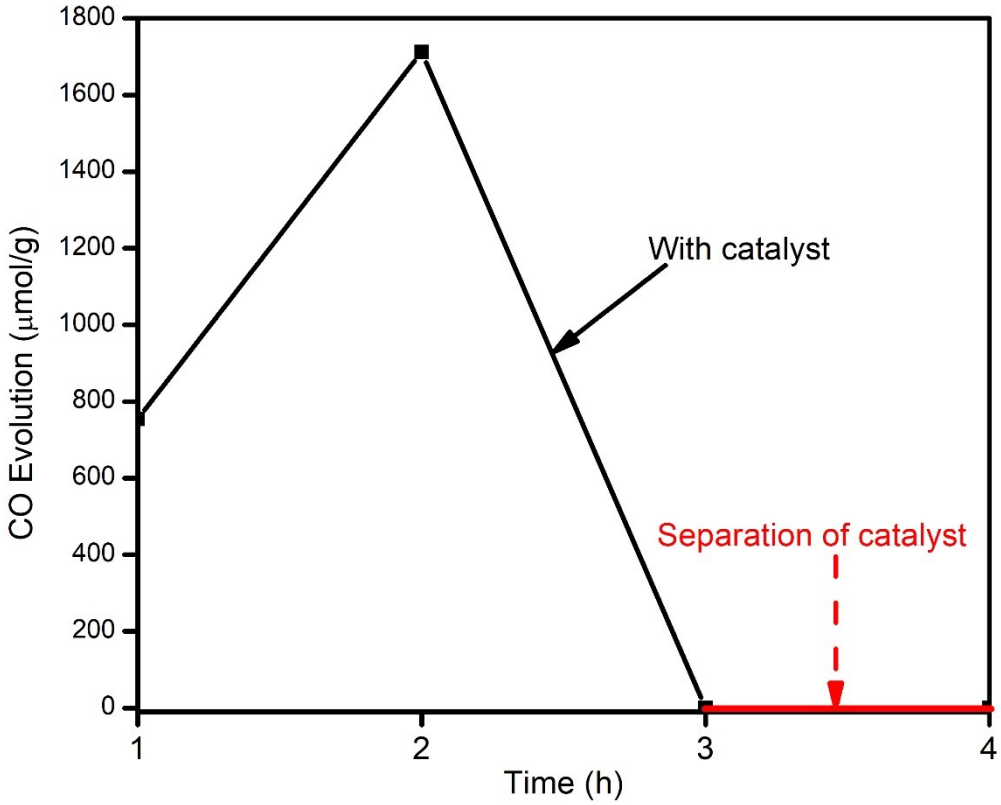


Fig. S19: Leaching test over CTF-TPE@Co-3.

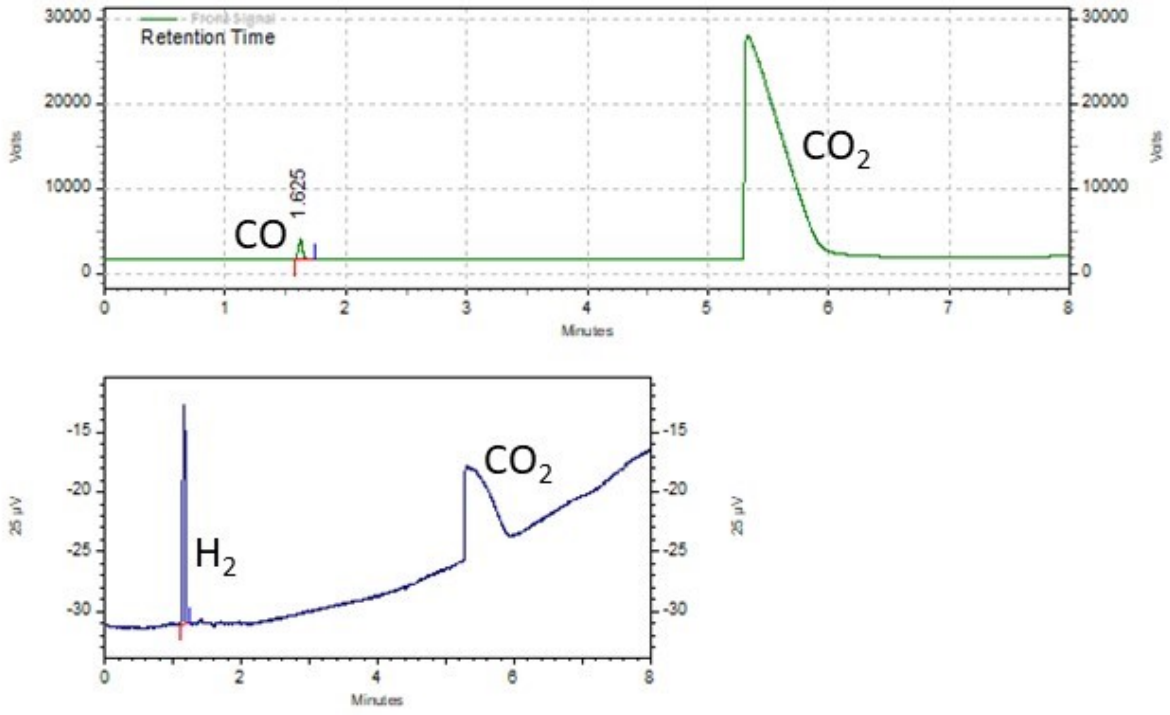


| Front Signal Results | | | | |
|---|---|---|---|---|
| Retention Time | Area | Area % | Height | Height % |
| 1.625 | 46667151 | 100.00 | 19057428 | 100.00 |
| Totals | | | | |
| | 46667151 | 100.00 | 19057428 | 100.00 |
| **Back Signal Results** | | | | |
| Retention Time | Area | Area % | Height | Height % |
| 1.167 | 310236 | 100.00 | 140757 | 100.00 |
| Totals | | | | |
| | 310236 | 100.00 | 140757 | 100.00 |

Fig. S20: Gas chromatogram of $CO_2$ reduction by CTF-TPE@Co-3.

**Liquid product quantification:** The liquid phase has taken from the reaction mixture after light irradiation for 7 hours. The solvent has been analysed through the ion chromatography (Fig. S21a) and $^1$H NMR spectroscopy (Fig. S21b). The ion chromatography results reveal negligible amount of formate (0.016 μmolg$^{-1}$). Meanwhile, the $^1$H NMR spectroscopy does not show any other liquid hydrocarbon products derived from $CO_2$ such as $CH_3OH$, $C_2H_5OH$, etc.

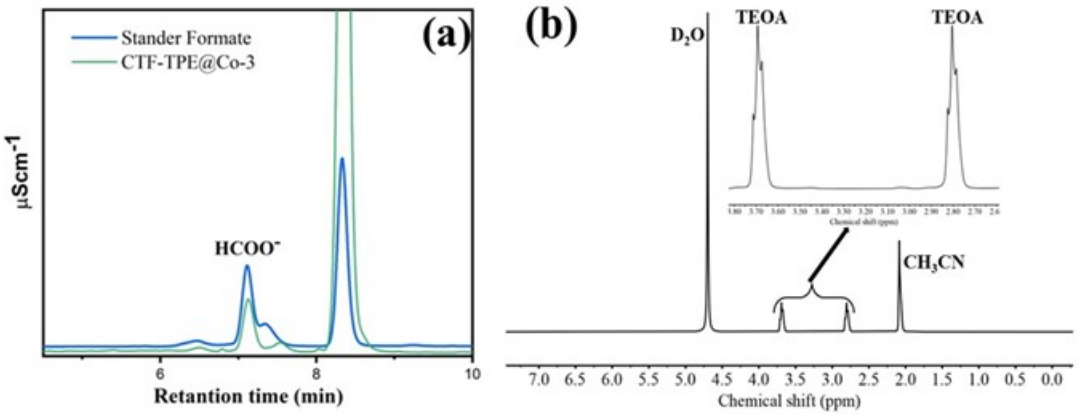


Fig. S21: (a) Ion chromatography curve and (b) $^1$H NMR spectra of liquid product after $CO_2$ reduction.

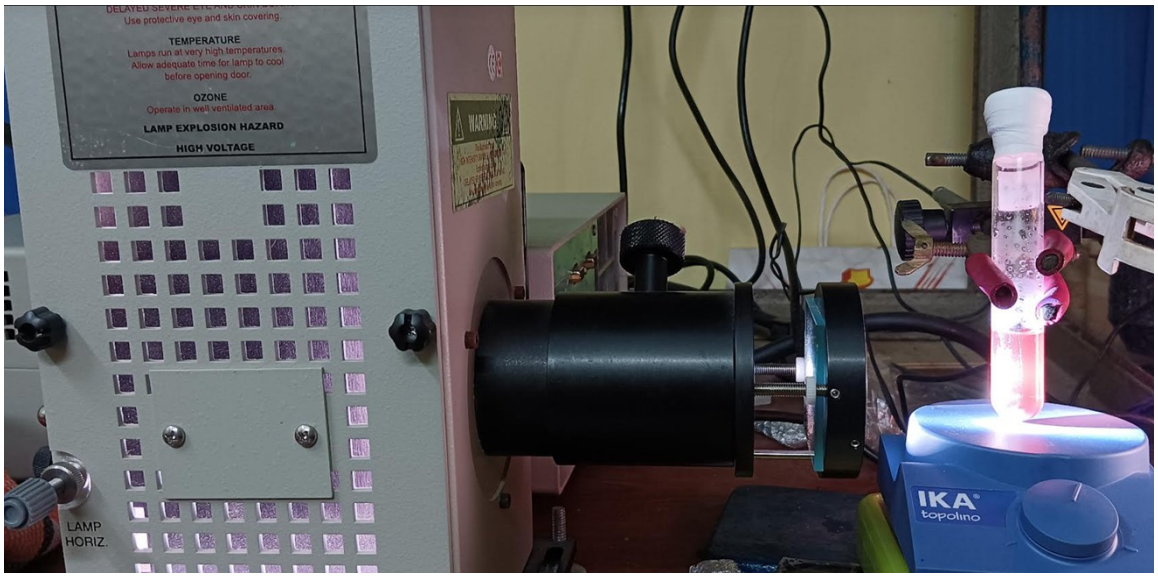


Fig. S22: Experimental set up of photocatalytic $CO_2$ reduction reaction.

Fig. S23: Experimental set-up and environment for sunlight-driven $CO_2$ reduction reaction (**Date: 27th April 2023, Cloudy weather**).

**Comparison of CO production by different photocatalyst:**

**Table S4. Comparison performance of photocatalytic CO evolution**

| **Photocatalyst** | **Illumination range** | **SA** | **PS** | **Product** | **Production rate[a]** | **Reference** |
|---|---|---|---|---|---|---|
| Ni-TpBpy-COF | λ > 420 nm | TEOA | $[Ru(bpy)_3]Cl_2$ | CO | 966 | 1 |
| TTCOF-Zn | 420 nm | $H_2O$ | - | CO | 2.06 | 2 |
| ACOF-1 | 420 nm | $H_2O$ | - | $CH_3OH$ | 60 | 3 |
| $N_3$-COF | 420 nm | $H_2O$ | - | $CH_3OH$ | 98.3 | 4 |
| Co-FPy-CON | 420 nm | TEOA | $(Ir[dF(CF_3)ppy]_2(dtbpy))PF_6$ | CO | 1681 | 5 |
| Co/CTF-1 | λ > 420 nm | TEOA | $[Ru(bpy)_3]Cl_2$ | CO | 50 | 6 |
| Re-CTF-py | 200 nm | TEOA | - | CO | 353.05 | 7 |
| CTF-TPN | λ > 420 nm | TEOA | - | CO | 330.3 | 8 |
| NCTF-1 | λ > 420 nm | TEA | - | $CH_4$ | 11.48 | 9 |
| $ZnFe_2O_4$/FeP-CTFs | λ > 420 nm | TEOA | $[Ru(bpy)_3]Cl_2$ | $CH_4$ | 178 | 10 |
| Pt-SA/CTF-1 | λ > 420 nm | TEA | - | $CH_4$ | 4.5 | 11 |
| $TiO_2$@CTF-Py | λ > 320 nm | $H_2O$ | - | CO | 43.34 | 12 |

| | | | | | | |
|---|---|---|---|---|---|---|
| $Ni(OH)_2$/CTF-1 | λ > 420 nm | TEOA | $[Ru(bpy)_3]Cl_2$ | CO | 38.66 | 13 |
| CPB/CTF-1-Ni | λ > 420 nm | EA | - | CO | 86.5 | 14 |
| $Fe_2O_3$@Por-CTF10 | λ > 420 nm | TEOA | $[Ru(bpy)_3]Cl_2$ | CO | 400 | 15 |
| **CTF-TPE@Co-3** | **λ > 420 nm** | **TEOA** | **$[Ru(bpy)_3]Cl_2$** | **CO** | **750** | **This work** |

## References:


1. W. Zhong, R. Sa, L. Li, Y. He, L. Li, J. Bi, Z. Zhuang, Y. Yu and Z. Zou, *J. Am. Chem. Soc.* 2019, **141**, 7615–7621.
2. M. Lu, J. Liu, Q. Li, M. Zhang, M. Liu, J.-L. Wang, D.-Q. Yuan and Y.-n. Lan, *Angew. Chem. Int. Ed.* 2019, **58**, 12392-12397.
3. Y. Fu, X. Zhu, L. Huang, X. Zhang, F. Zhang and W. Zhu, *Applied Catalysis B: Environmental*, 2018, **239**, 46-51.
4. A. F. M. EL-Mahdy, H. A. E. Omr, Z. A. Alothman and H. Lee, J. Colloid Interface Sci., 2023, **633**, 775-785.
5. X. Wang, Z. Fu, L. Zheng, C. Zhao, X. Wang, S. Y. Chong, F. McBride, R. Raval, M. Bilton, L. Liu, X. Wu, L. Chen, R. S. Sprick and A. I. Cooper, *Chem. Mater.* 2020, **32**, 9107–9114
6. J. Bi, B. Xu, L. Sun, H. Huang, S. Fang, L. Li and L. Wu, *ChemPlusChem*, 2019, **84**, 1149-1154
7. R. Xu, X.-S. Wang, H. Zhao, H. Lin, Y.-B. Huang and R. Cao, *Catal. Sci. Technol*., 2018, **8**, 2224-2230.
8. Y. He, X. Chen, C. Huang, L. Li, C. Yang and Y. Yu, *Chin*. *J. Catal.,* 2021, **42**, 123-130.
9. Q. Niu, Z. Cheng, Q. Chen, G. Huang, J. Lin, J. Bi and L. Wu, *ACS Sustainable Chem. Eng.*, 2021, **9**, 1333-1340.
10. Y. Yan, Q. Fang, J. Pan, J. Yang, L. Zhang, W. Zhang, G. Zhuang, X. Zhong, S. Deng and J. Wang, *Chem. Eng. J.,* 2021, **408**, 127358.
11. G. Huang, Q. Niu, J. Zhang, H. Huang, Q. Chen, J. Bi and L. Wu, *Chem. Eng. J.,* 2022, **427**, 131018.
12. Z. Xu, Y. Cui, D. Young, J. Wang, H. Li, G. Bian and H. Li, *J. $CO_2$ Util*., 2021, **49**, 101561
13. T. Zhao, Q. Niu, G. Huang, Q. Chen, Y. Gao, J. Bi and L. Wu, *J. Colloid Interface Sci.*, 2021, **602**, 23-31.
14. H. Zhong, Z. Hong, C. Yang, L. Li, Y. Xu, X. Wang and R. Wang, *ChemSusChem,* 2019, **12**, 4493-4499.
15. S. Zhang, S. Wang, L. Guo, H. Chen, B. Tan and S. Jin, J. *Mater. Chem. C*, 2020, **8**, 192-200.